Nonlinear dynamic analysis of a large-scale single-layer latticed dome with uncertainties of damping and geometric shape

Hui-dong Zhang,[1,2] Xin-qun Zhu,[3] Guo-ji Liu,[1] and Guo-ping Liu[1]

[1]Tianjin Key Laboratory of Civil Buildings Protection and Reinforcement, Tianjin 300384, PR China

[2]School of Civil Engineering, Tianjin Chengjian University, Tianjin 300384, PR China

[3]School of Civil and Environmental Engineering, University of Technology Sydney, Broadway, NSW 2007, Australia

Correspondence should be addressed to Hui-dong Zhang; zhhuidong@126.com

Abstract: Most of current evaluations for structural design are based on deterministic analysis. In practice, the parameters of the structure such as material, mass distribution, imperfections and damping have uncertainties. this will affect the final evaluations and structural safety if the deterministic analysis method is still used. The conventional method has to be improved. Therefore, there is an increasing need for evaluating the structural performance with the uncertainty analysis method. In this study, a method is developed and presented for the dynamic uncertainty analysis of a large-scale single-layer lattice dome. The method can take into account the uncertainties of the damping, the material, the structural mass or load, and the geometry imperfections of the structural shape and all members. It is implemented by assuming that the variability of each random input parameter with respect to the ideal parameters of the perfect structure obeys a mathematical distribution. Specifically, there is a basic difference between the present study and other related studies on treatments of uncertainty in damping. After a computer model of the dome with the geometry imperfections of the structural shape and all members is constructed, finite element dynamic analyses with uncertainties of damping and input parameters are performed. Additionally, the mathematical distributions of dynamic properties and demands are analyzed. Results show that the variability of the parameters with an associated uncertainty imposes significant negative effects on the dynamic performance of the dome, and the probability of failure of the dome increases as increase of variability levels of uncertain parameters, indicating that reducing the uncertainty of the input parameters has a significant contribution to the safety of a dome. By comparison, a significant difference in the dynamic demands is observed when the uncertainty analysis method and conventional analytical method are respectively used for the dynamic analysis; the numerical results reveal the necessity for the use of the proposed method in practical applications.

Keywords: random dynamic analysis; damping uncertainty; imperfections; single-layer lattice dome; computational analysis

1. Introduction

In accordance to the current building design practice and guidelines, most design evaluations are based on deterministic values. However, numerous prior research studies [1–3] have indicated that the uncertainties in design evaluations can be quite significant. In recent years there has been increased attention in the use of uncertainty analysis (UA) for the evaluation of structural performance [4–6].

It is commonly assumed that an uncertainty can be classified into two categories [7, 8]: *aleatoric* uncertainty and *epistemic* uncertainty. In general, in a specific structure, the uncertainties can be related to the materials used, the geometry, structure, and loads [9].

At the material level, over all physical and mechanical properties that a material exhibits, mass and stiffness usually are fairly close to their nominal values, unlike strength, which depends strongly on chemical composition and heat treatment. However, the elastic modulus is a particularly important parameter among these mechanical properties, and the material strength and the instability failure modes of structures rely heavily on this parameter [9]. It is observed by experimental tests that the parameter has an important variability, and the statistical analysis indicated that the normal or lognormal distribution matched closely the experimental test data [10]. The results [11] showed that the variation of elastic modulus mostly affected the behavior of the structure during the elastic region and changed the deformation

demands.

At the member level, the members in a steel structure are commonly analyzed assuming that the members are perfectly straight between joints. However, no member is perfectly straight in a manufacturing process, the initial imperfection always exists, and its quantification is random and uncertain. However, it should be noted that the mechanical behaviors of the steel members are very sensitive to the initial imperfections [12, 13]. Many researchers [10, 14–16] have investigated the influence of the initially random imperfection on the load-carrying capacity of a member, and pointed out that the initial imperfections led to the reduction of the load-carrying capacity of the member under compression or/and bending due to second order phenomena ($P-\delta$ effect). In terms of modeling the initial imperfection of the steel member, AISC-2010 [17] considers that it shall be taken into account either by direct modeling or by the application of *notional loads,* as specified in this standard. However, more researchers [18, 19] considered that the initial imperfection should be directly modeled, and that the random approach, instead of statistical approach, is more reasonable.

Uncertainties of structural shape may typically arise from imprecision during the process of manufacturing or construction or round-off errors [20]. This leads to inexact joint positions during construction. The existence of such random errors reduces the structural stiffness. However, these errors cannot be avoided, and their quantification is random. It was observed in previous studies [6, 21] that the variance of nodal coordinates may be an important source of uncertainty in structural reliability, particularly when nonlinear structural behavior is considered [21]. Therefore, the conventional deterministic analysis for a structure may lead to inaccurate results. proposed analytical methods for structures with a small uncertainty in nodal locations have reported [20, 22].

Loads in structures are the important source of uncertainty in the evaluation of structural performance. These loads mainly include the dead load and the live load. The wind load and seismic load belongs to external excitations, which are not discussed in this study. For internal loads, their stochastic models and characteristics depend on many factors, such as the shape of the structure, distribution of different materials, and the precision in the construction process. The dead load comprises the weights of the structural elements and nonstructural items, but the uncertainty in the weights of nonstructural items only is the main source of the dead load variability [23]. Therefore, dead loads usually have minimal uncertainties. For live loads, a limited number of load surveys were conducted to estimate the statistics relevant to the live load [24, 25]. It was observed that in the vast majority of cases, live loads are the primary contributors to the uncertainties of loads [26]. In general, the dead load is normally distributed and the live load has a Gumbel (extreme value type I) distribution [23]. Therefore, the deterministic method for describing the properties of the loads need to be improved.

In terms of damping, numerical results show that the damping value selected has a significant effect on the dynamic demands, especially for lightly damped structures [27]. However, in engineering practice, damping is very difficult to identify and quantify due to its complex nature, the estimation of structural damping depends on a wide range of factors. The scatter test data from real buildings, quantification techniques of damping, and even the occasional misuse of measurement techniques, lead to the intrinsic variability of the damping. At present, although there are empirical formulas to predict the total damping of a structure, those formulas may result in an unacceptable scatter in damping values [28]. As pointed out by Kareem [29], quantification of damping is by far the most vexing problem in structural engineering.

Beyond all the listed aspects relevant to a structure, there are significant sources of uncertainty. Modeling uncertainties of these sources are one of the most challenging topics in the seismic assessment of existing buildings. The objective of this paper is to investigate how the treatment of the different sources with randomness and uncertainty will affect the assessment of structural performance. The following primitive variables for a large-scale single-layer lattice dome subjected to dynamic loads are considered in this paper: (1) elastic modulus of material, (2) mode damping ratio, (3) shape imperfection (nodal coordinates), (4) initial imperfections of members, and (5) roof mass distribution. In the

finite element dynamic analyses, the primitive variables vary randomly and simultaneously. The mathematical distributions of the dynamic demands and the dynamic performance of the dome are investigated.

2. Damping in structures

2.1Material damping

2.1.1 A hysteretic material model for modeling material damping

The Bouc–Wen model is a smooth hysteretic model [30]. The model is often used to describe nonlinear hysteretic systems subjected to different excitations due to its ability to represent a wide range of hysteresis loop shapes. However, it is rarely used in simulating hysteretic behaviors in materials, and this is mainly because of a lack of a thorough understanding for material damping.

The nonlinear material stress–strain relationship of the Bouc–Wen model is expressed as [30],

$$\sigma = \alpha E\varepsilon + (1-\alpha)Ez \tag{1}$$

where σ is the stress, ε is the strain, z represents the hysteretic deformation, E is the elastic modulus, and α is the ratio of post-yielding to elastic modulus. The model defines the hysteretic behavior as the sum of a linear part and a hysteretic part. The first part represents the participation level of the initial stiffness into the inelastic response of the oscillator, whereas the latter part accounts for the nonlinear hysteretic characteristic with memory of previous loading cycles by means of the hysteretic deformation, z. The model was improved by Baber and Noori [31] to account for degrading behaviors by introducing the rate of hysteretic deformation, $\dot{z}$,

$$\dot{z} = \frac{A\dot{\varepsilon} - \left\{\beta\left|\dot{\varepsilon}\right|z\left|z\right|^{n-1} + \gamma\dot{\varepsilon}\left|z\right|^{n}\right\}\nu}{\eta} \tag{2}$$

where $\dot{\varepsilon}$ is strain rate, β, γ, and n, are parameters that control the shape of the hysteretic loop. In this model, A, ν, and η, are variables that control the degradation process in stiffness and strength.

Eq. (2) can also be rewritten as,

$$\dot{z} = \frac{A - \left|z\right|^{n}\left\{\beta\,\mathrm{sgn}(\dot{\varepsilon}z) + \gamma\right\}\nu}{\eta}\dot{\varepsilon} \tag{3}$$

Using Eqs. (1) and (3), the following expression can be obtained,

$$\frac{\partial\sigma}{\partial\varepsilon} = \alpha E + (1-\alpha)E\,\frac{A - \left|z\right|^{n}\left\{\beta\,\mathrm{sgn}(\dot{\varepsilon}z) + \gamma\right\}\nu}{\eta} \tag{4}$$

Depending upon the memory of past cycles, the degradation process is introduced by the following expressions [30],

$$\begin{cases} A = A_o - \delta_A e(t) \\ \nu = 1 + \delta_\nu e(t) \\ \eta = 1 + \delta_\eta e(t) \end{cases} \tag{5}$$

where $e(t)$ is the hysteretic energy up to the specific time t, and A_o, δ_A, δ_ν, and δ_η, are user-defined parameters.

It has been found that the parameters of the Bouc–Wen model are functionally redundant. Eliminating this redundancy is best achieved by setting $A = 1$ [32]. Herein, n is usually greater or equal to 1, and as n increases, the transition from the elastic range to the inelastic range becomes sharper. The parameter β is positive by assumption, while the admissible values $\gamma \in [-\beta, \beta]$. In the Bouc–Wen model, softening behavior occurs when (a) $\beta + \gamma > 0$ and $\beta - \gamma > 0$, (b) $\beta + \gamma > 0$ and $\beta - \gamma < 0$, and (c) $\beta + \gamma > 0$ and $\beta - \gamma = 0$. In this model, the dynamic behavior is governed by several parameters, which are determined using experimental data.

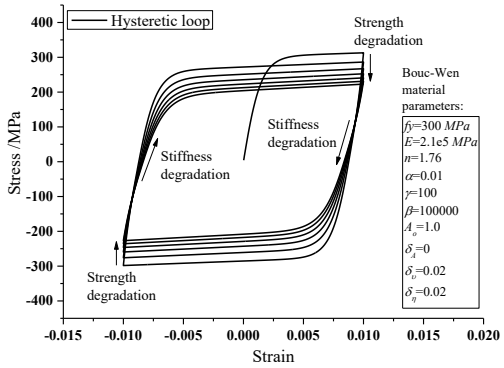

Fig. 1 Hysteretic behavior of the Bouc–Wen steel material and its degradation

An example on the hysteretic behavior exhibited by the application of the Bouc–Wen model for steel materials is illustrated in Fig. 1. The material parameters are obtained from the literature [3], and are based on experimental test data. In this example, the strength and stiffness degradation in the steel material is shown after each loading cycle. Most of the previous literature studies that considered the nonlinear behavior of materials used nondegrading hysteretic models subjected to repeated cyclic load reversals, such as earthquakes. Consequently, this may have led to an overestimation of the steel material performance. In this paper, these degradation properties of the steel material are directly considered in dynamic analyses.

2.1.2 Quantification of material damping

For steel materials, dislocation slip occurs when the materials are subjected to cyclic stresses, even under very low stress levels, and this leads to internal material friction and energy loss (or alternatively, to a material damping effect). In previous literature studies, the material damping was usually incorporated into the global damping using an approximate estimation of the material damping ratio, depending on the vibration frequency. However, in a physical sense, the energy loss due to the internal friction of materials can be directly described by means of material constitutive models that consider internal friction effects, such as the Ramberg–Osgood or the Bouc–Wen material models [33]. As stated previously, these hysteretic models merged a linear component and a nonlinear component in parallel, regardless of the elastic and plastic ranges. The nonlinear component is owing to the internal friction of the material in the elastic range. Thus, in this paper, another advantage in the use of the Bouc–Wen model to the modeling of steel materials is that it is able to capture the material damping, even in the elastic range of the material, as illustrated in Fig. 2. It is clearly observed that for steel materials subjected to cyclic loading, hysteresis occurs and induces the damping effect.

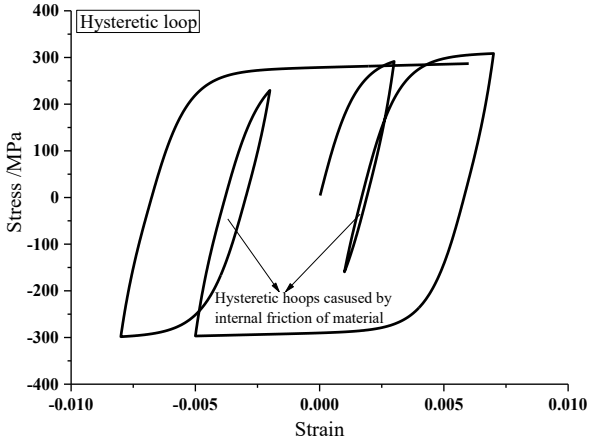

Fig. 2 Hysteretic loops of steel based on the Bouc–Wen model

These stress–strain hysteretic loops can be used to quantify the material damping ratios in accordance to,

$$\xi_{eq} = \frac{\eta}{2} = \frac{1}{4\pi}\frac{E_D}{E_s} \tag{6}$$

where ξ_{eq} is the equivalent material damping ratio, η is the material loss factor, E_D is the dissipated energy of the material, and E_s is the maximum strain energy of the material, $E_s = \sigma^2/(2E)$. For metallic materials, the specific damping energy of material D is a function of stress, as stated by Goodman [34].

$$D = J\left(\frac{\sigma}{\sigma_e}\right)^n \tag{7}$$

where J and n are the material constants, σ is the material stress level in a cycle, and σ_e is the fatigue limit. Usually, the exponent n is equal to 2.4. Substituting Eq. (7) into Eq. (6), leads to

$$\xi_{eq} = C\sigma^{n-2} \tag{8}$$

where C is a material constant that is associated with the fatigue limit. From Eq. (8), it can be seen that the relationship between the material damping ratio and the material stress is nonlinear. However, when $n = 2$ the equivalent material damping ratio, ξ_{eq}, is constant.

According to Eq. (6), ξ_{eq} can be calculated under different material stress levels in the elastic range, as shown in Fig. 3. Evidently, as the material stress increases, the material damping ratio increases nonlinearly instead of being frequency-dependent. The relationship between the equivalent material damping ratio and the material stress can be obtained by fitting these discrete data,

$$\xi_{eq} = 9.126e-7\sigma^{2.176} \tag{9}$$

where σ is the material stress. In Eq. (9), the exponent is equal to 2.176, and equivalently, in Eq. (8), the exponent n is 4.176. This equation is very important for estimating the material damping ratio in engineering practice. However, when the material reaches a high stress level, which is lower than the yielding strength of the material, such as 200 *MPa*, the material damping ratio is nearly equal to 10%. It should be noted that the material damping ratios of a member or structure are far below these values because the stress in a member or structure is non-uniformly distributed. Therefore, it could not simultaneously reach the high stress in all parts of a member or structure. The material damping ratio of a single-layer lattice dome subjected to earthquake ground motions have been evaluated by Zhang *et al.* [35]. In their study, they showed that the material damping ratio of a dome is approximately 0.5%. Although the value is small, it approximately accounts for 20% of the total damping in the dome.

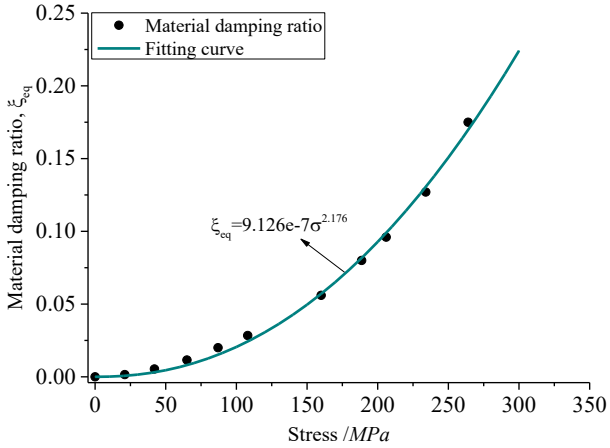

Fig. 3 Material damping ratio of steel under different stress levels

2.1.3 Uncertainty of material damping

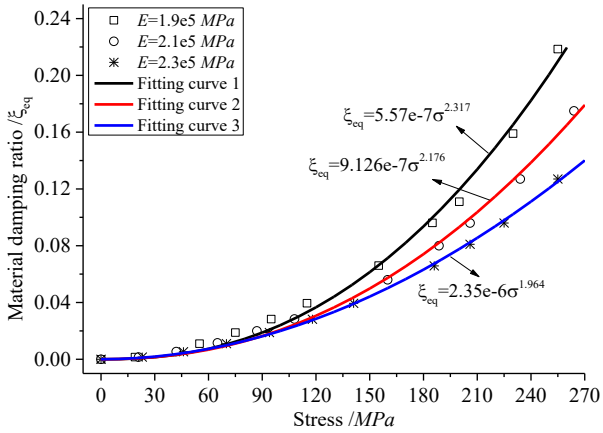

Fig. 4 Damping ratios of materials at different elastic moduli

According to Eqs. (1) and (9), it can be seen that the elastic modulus E has a direct effect on the material damping ratio. As stated previously, because the material parameter E has a significant variability instead of a constant value, this gives rise to the variability of the material damping ratio. Through sensitivity analyses, the effects of this material parameter on the material damping ratios are presented in Fig. 4. It is observed that the effect of the elastic modulus on the material damping ratio are obvious at middle and high stress values, and that the reduction of the elastic modulus can increase the material damping. With the increase of material stress, the trend is more notable. Moreover, it can also be seen in this figure that the exponent in Eq. (8) deceases, and that the constant C increases with the increase of the elastic modulus. Additionally, the exponent value is approximately between 1.9 and 2.3. Therefore, it can be concluded that the material damping ratio is approximately proportional to the square of the material stress when the Bouc-Wen material model is used.

2.2 Structural damping

2.2.1Modeling structural damping using the Rayleigh damping model

The energy dissipation of a structure subjected to earthquakes is from three main sources, namely, the energy radiation, nonlinearity of the material, and inherent damping. The energy radiation exists at the supports of the structure. While the nonlinearity of the material can dissipate part of the energy through plastic deformation, the internal friction of the material in the inherent damping can be captured by means of the material constitutive model. However, the inherent damping, such as the Coulomb frictions in joint connections of a structure, and between members and nonstructural components, and in other frictional mechanisms, is still unidentified. For these unquantifiable damping sources, the Rayleigh damping model is commonly used to implicitly represent their energy dissipations. Although the physical or rheological meaning of this approach is not clear, it is a very convenient way of accounting for damping for numerical solution purposes [36].

2.2.2 Calculation of damping coefficients

The form of Rayleigh damping is in accordance to the following equation,

$$C = \alpha M + \beta K \tag{10}$$

where M and K are the mass and stiffness matrices, respectively, C is the damping matrix, and α and β are the mass and stiffness damping coefficients, respectively. According to Eq. (10), the damping ratio of the i^{th} mode is,

$$\xi_i = \frac{\alpha}{2\omega_i} + \frac{\beta\omega_i}{2} \tag{11}$$

The coefficients α and β can be determined from the specified damping ratios, ξ_m and ξ_n, for the m^{th} and n^{th} modes, respectively. Usually, assuming that ξ_m=ξ_n=ξ, yields

$$\begin{cases} \alpha = \dfrac{\omega_m \omega_n}{\omega_m + \omega_n} 2\xi \\ \beta = \dfrac{1}{\omega_m + \omega_n} 2\xi \end{cases} \tag{12}$$

In Eq. (12) the coefficients are defined using two modes only. After that, other mode damping ratios are estimated by these coefficients. This may lead to a very large error. In order to reduce the error, the Least Squares Method (LSM) is used to obtain the damping coefficients. According to Eq. (11), the following expression can be derived,

$$\Delta\sigma_x = \sqrt{\frac{1}{n}\sum_{i=1}^{n}\left(\frac{\alpha}{2\omega_i} + \frac{\beta\omega_i}{2} - \xi_i\right)^2} \tag{13}$$

where $\Delta\sigma_x$ is the standard deviation. When $\Delta\sigma_x$ attains its minimum value, the best fitting curve of the frequency-damping ratios can be obtained. Define the function, $\Gamma(\alpha,\beta)$,

$$\Gamma(\alpha,\beta) = \sum_{i=1}^{n}\left(\frac{\alpha}{2\omega_i} + \frac{\beta\omega_i}{2} - \xi_i\right)^2 \tag{14}$$

In order to obtain the values of α and β, let the partial derivatives of $\Gamma(\alpha,\beta)$ with respect to α and β be equal to zero,

$$\begin{cases} \dfrac{\partial\Gamma}{\partial\alpha} = \dfrac{\alpha}{2}\displaystyle\sum_{i=1}^{n}\frac{1}{\omega_i^2} - \sum_{i=1}^{n}\frac{\xi_i}{\omega_i} + \frac{n\beta}{2} = 0 \\ \dfrac{\partial\Gamma}{\partial\beta} = \dfrac{\beta}{2}\displaystyle\sum_{i=1}^{n}\omega_i^2 - \sum_{i=1}^{n}\omega_i\xi_i + \frac{n\alpha}{2} = 0 \end{cases} \tag{15}$$

Solving Eq. (15), yields the following solutions,

$$\begin{cases} \alpha = \dfrac{2\left(\displaystyle\sum_{i=1}^{n}\frac{\xi_i}{\omega_i}\sum_{i=1}^{n}\omega_i^2 - n\sum_{i=1}^{n}\omega_i\xi_i\right)}{\displaystyle\sum_{i=1}^{n}\frac{1}{\omega_i^2}\sum_{i=1}^{n}\omega_i^2 - n^2} \\ \beta = \dfrac{2\left(\displaystyle\sum_{i=1}^{n}\omega_i\xi_i\sum_{i=1}^{n}\frac{1}{\omega_i^2} - n\sum_{i=1}^{n}\frac{\xi_i}{\omega_i}\right)}{\displaystyle\sum_{i=1}^{n}\frac{1}{\omega_i^2}\sum_{i=1}^{n}\omega_i^2 - n^2} \end{cases} \tag{16}$$

In order to present the accuracy of the LSM, an example is illustrated next. According to the first 20 frequencies and mode damping ratios listed in Table 1, the frequency-damping ratio curves predicted by means of the conventional method and LSM are compared, as illustrated in Fig. 5. It is observed that only two damping values lie on the curve with the conventional method, whereas most of values lie below the curve. This leads to an overestimation of the damping ratios in a structure. However, the estimation values based on LSM exhibit a good agreement with the real data, and the real values are very near the estimation curve. It is apparent that the LSM yields better results than the conventional method in terms of estimating the damping values.

Table 1 Frequency versus the damping ratio

Mode	1	2	3	4	5	6	7	8	9	10
Frequency /Hz	2.96	2.97	3.20	3.20	3.227	3.24	3.268	3.268	3.289	3.29
Damping ratio	0.0148	0.0146	0.0147	0.0147	0.0147	0.0147	0.0147	0.0147	0.0148	0.0148

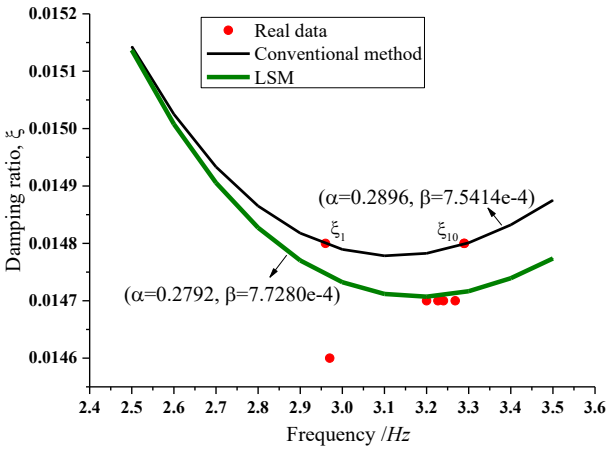

Fig. 5 Frequency-damping ratio curves using different methods

2.2.3 Uncertainty of structural damping

In reality most structures behave nonlinearly with the increase of the amplitude of the input force. However, existing damping evaluation techniques are based on linear system theories. When linear identification methods are applied to nonlinear dynamic properties, an equivalent linear method has to be employed. It should be noted that this equivalence may cause remarkable errors. In general, at present, the accuracy of the estimated damping is much lower than that of the estimated natural frequencies and mode shapes. There is an example from field experiments to present the uncertainty of mode damping ratios in identification precision, as listed in Tables 2 and 3.

Table 2 Damping ratios evaluated by the multimode random decrement (MRD) method and the frequency domain decomposition (FDD) method [37, 38]

	MRD	FDD	error
Mode 1	0.18%	0.24%	33%
Mode 2	0.30%	0.39%	30%
Mode 3	0.83%	0.30%	-64%
Mode 4	0.85%	0.91%	7%
Mode 5	0.55%	0.65%	18%

Table 3 Estimated damping ratios and FFT data points [37, 38]

	256	512	1024	2048	4096	8192
Mode 1	3.05%	1.60%	0.95%	0.65%	0.54%	0.51%
Mode 2	2.81%	1.58%	0.99%	0.74%	0.67%	0.58%
Mode 3	2.06%	1.29%	0.98%	0.84%	0.80%	0.87%
Mode 4	1.52%	1.24%	1.11%	1.10%	1.08%	1.06%
Mode 5	1.91%	1.64%	1.65%	1.56%	1.62%	1.29%

According to Table 2, it is observed that the estimated damping ratios of different modes with different

identification methods have significant differences. The reason is that the equivalence of a nonlinear system to a linear system is approximate and the error is unavoidable, as stated previously. The FFT data points have a remarkable effect on the estimations of the damping ratios, as it can be seen in Table 3. These result in a high variability and low stability in the damping values. According to the experimental validation [39], it was found that the mode damping ratio has a Gaussian (or normal) distribution. A fundamental purpose in identifying the damping ratios of a structure is for using these values to construct the damping matrix. Due to the uncertainty of the damping ratios, the damping matrix is inaccurate.

3. Random imperfections in a structure

3.1 Imperfection of the structural shape

The positions of connections define the geometry of a structure. However, due to the construction errors the positions of connections are inexact. Correspondingly, this causes variability in the shape of structural geometry. Because the errors are random, the structural geometry shape has randomness. In the present paper, the imperfection is created by considering only the degrees of freedom of global translation (but not the rotation) of the end-joints of a member. The variations of nodal coordinates of a joint are introduced using random variables, and are added to the ideal nodal coordinates. Assume that the i^{th} joint has randomness in its location, and then its coordinates can be expressed as,

$$\{XYZ_i\}^{imp} = \{XYZ_i\}^0 + \{R_i\} \tag{17}$$

where $\{XYZ_i\}^{imp}$ are the nodal coordinate vectors with construction errors, in which i=1, 2, and 3, respectively represent the x, y, and z directions, $\{XYZ_i\}^0$ are the nodal coordinate vectors without imperfections, and $\{R_i\}$ are the random error vectors of the nodal coordinates, which are respectively randomly generated with a normal distribution that has a zero mean and specified standard deviations along the x, y, and z directions. The random errors herein are considered to be uncorrelated.

3.2 Member imperfections

Initial deflection, initial eccentricity and residual stress are unavoidable in practical members, and must be considered in dynamic analyses. However, these imperfections cannot be directly measured. To describe these imperfections, most standards recommend an equivalent imperfection, based on the use of a half wave for all member imperfections, which are equivalently translated into the initial deflection. This is implemented by adding a finite element node at the mid-span of a member, as shown in Fig. 6, in which nodes 1 and 2 are the end-joints of the member. The initial position of node 3 is located at the mid-span of the member. It should be noted that nodes 1 and 2 have been assigned coordinate deviations due to construction errors. Subsequently, through the control of the coordinates of the finite element node 3, the equivalent initial deflection of the member, δ, can be defined to be normally distributed with a zero mean and specific standard deviations along the x, y, and z directions. Herein, the deflection is considered as an independent random variable.

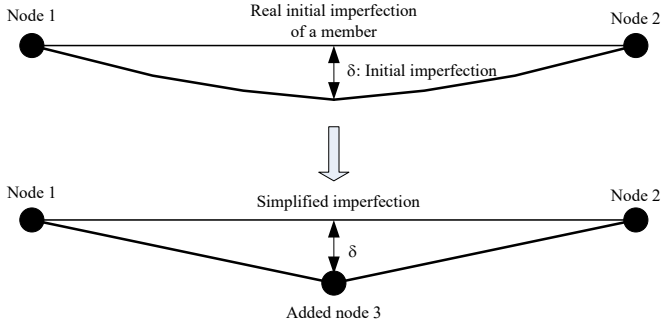

Fig. 6 Implementation of the equivalent initial deflection

4. Uncertainty analysis method for structures

In order to incorporate relevant sources of uncertainties of random input parameters, a fully probabilistic method coupled with nonlinear dynamic analysis provides a more realistic way to evaluate structural safety. Unlike the traditional deterministic analysis, structural probabilistic analysis treats these inputs as samples from probability distributions.

The cumulative distribution function (CDF) of a continuous random variable, $F(x)$, and the probability density function (PDF), $f(x)$, are defined as

$$F(x) = P[X \le x]$$
$$f(x) = \frac{dF(x)}{dx} \tag{20}$$

where X is random variable, x is specific value of the random variable, and $P[\cdot]$ is the probability of the variable listed inside the square brackets.

For the elastic modulus, the damping ratio of each mode, for all imperfections and the dead load, are considered as independent random variables and are normally distributed. The PDF of a normal distribution can be expressed as

$$f(R) = \frac{1}{\sigma_s \sqrt{2\pi}} \exp\left(\frac{(R-\mu)^2}{2\sigma_s^2} \right) \tag{21}$$

where R is the random variable, μ is the mean of R, and σ_s is the prescribed standard deviation of the random variable.

For a live load, the PDF can be described by a Gumbel distribution (extreme value type I),

$$f(x) = \frac{1}{\beta} \exp\left(\frac{x-\mu}{\beta} - \exp(\frac{x-\mu}{\beta}) \right) \tag{22}$$

where x is the random variable, μ is the location parameter of x, and β is the scale parameter ($\beta > 0$).

Recent developments using a Monte Carlo Simulation (MCS) technique have resolved many of the problems in the analysis of uncertainty. The computational process, however, is lengthy and expensive. The first- and second-order reliability methods (FORM and SORM) can be carried out for uncertain analyses [40, 41]. However, the FORM and SORM may give rise to numerical convergence in the reliability analysis for nonlinearity [42]. In order to reduce the calculation workload and avoid the numerical convergence, in this paper, the fitting techniques for the data from limited sampling are used in order to compute the probability of failure. Therefore, in the present case, the procedure is as follows:

Step 1: The random elastic modulus, imperfections, and loads, are respectively assigned to a mathematical distribution according to Eqs. (21) and (22), and the numerical model is updated

Step 2: A sequence of damping ratios of modes are generated, and the damping coefficients in the Rayleigh damping model are then solved using Eq. (16)

Step 3: The performance function of the dynamic demand is defined and a sampling size, $Ntrials$, is given.

Step 4: The static analysis is carried out, and the external excitations are then applied to the structure, thereby solving the value of the performance function $g(i)$ of each sample, until a specified number of analysis steps, $Ntrials$, is completed. The probability distribution of $\{g(i)\}$ can then be obtained using fitting technique.

Step 5: Finally, according to the probability distribution of $\{g(i)\}$, the probability of failure of the structure can be approximately estimated with an integral.

5. Illustrative example

5.1 Descriptions of the structure and analytical model

A numerical example is presented to illustrate the methodology described in this paper, and to quantify the influence of uncertainties of input parameters on the overall dynamic demands of a structure. The single-layer lattice dome that is subjected to dynamic excitations shown in Fig. 7, is taken as the basic model for the computations.

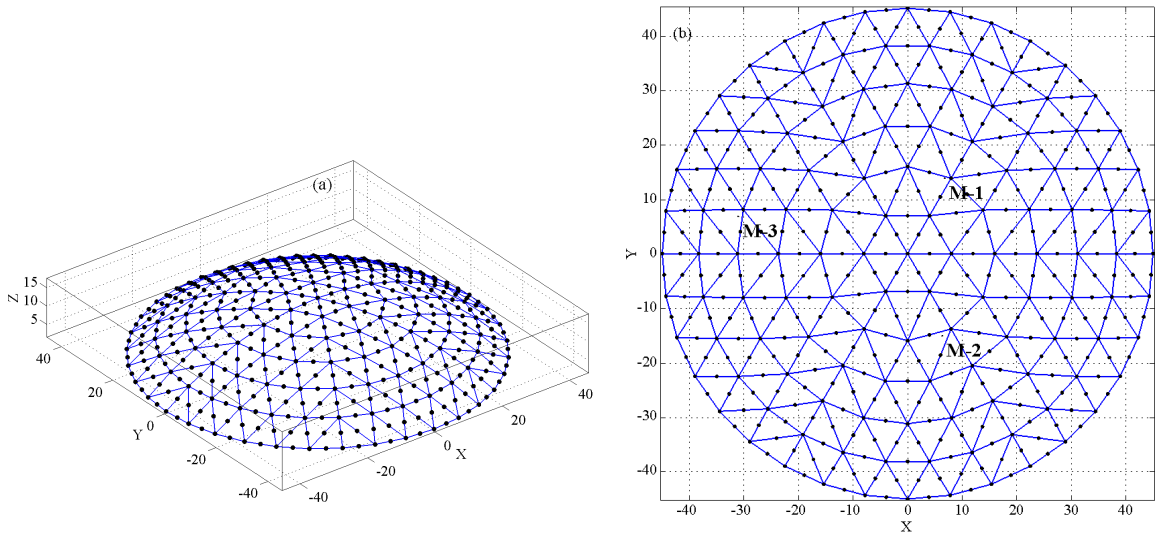

Fig. 7 Dome schematics without imperfections

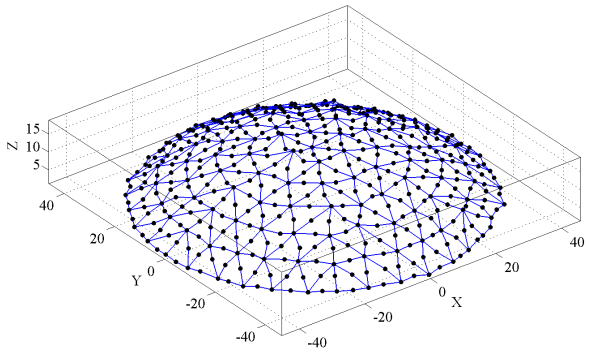

Fig. 8 A dome with imperfections

The 3D sophisticated numerical model is developed in OpenSees. Its span and height are 90 m and 15 m, respectively. In the dome, the lengths of the members range between 7.844 m and 10.81 m. The members used are steel tubes with an external diameter of 0.32 m and a wall thickness of 0.01 m. The uniform roof dead load is 90 kg/m^2 and the live load is 36 kg/m^2, and they are assumed to be concentrated at the joints as masses. The Bouc–Wen model is selected to model the nonlinear material behaviors, and the material parameters used for the perfect dome are shown in Fig. 1. The dome with joint construction errors and initial imperfections of members is randomly generated, as shown in Fig. 8. In this case, the errors and imperfections are normally distributed with a zero mean and standard deviations of 0.5 m and 0.2 m, respectively.

In the model, the *force-based beam-column* element is used to model the nonlinear behavior of members. However, compared with the *displacement-based beam-column* element, the torsional stiffness of the section needs to be supplemented. To be able to observe buckling of a member, each member is divided into two inelastic elements. Each element has five *Gauss* integration points along the element length to describe the dynamic behaviors of the element. The section of each tube is dispersed into 20 fiber areas along the hoop, and into five layers along the radial direction. These treatments are sufficient for an accurate result on a hysteretic buckling behavior of the member, and on estimating the stress–strain distribution on steel tube sections. The *corotational coordinate transformation* object is

constructed, which performs a geometric transformation of stiffness of the member and the resisting force from the basic system to the global coordinate system. Given that the imperfections of the dome are very small compared to the sizes of members, it should be noted that in this paper the geometric transformation vectors of each element in the dome with imperfections are approximated with those of the perfect dome.

A failure criterion using the vertical response quantity d at the top is prescribed in terms of a performance function $g(\hat{d}, d)$. A negative outcome of the function, $g \leq 0$, is defined as a failure. In this paper, the performance function employed is expressed by a threshold and a response quantity in the form,

$$g(\hat{\mathrm{d}}, \mathrm{d}) = \hat{\mathrm{d}} - \mathrm{d}(\{\mathrm{x}_i\}) \tag{23}$$

where $\hat{d}$ is the threshold, and $d(\{x_i\})$ is the maximum vertical dynamic response at the top in the time series of each sampling, and x_i is the random variable. In reliability problems, the probability of failure, P_f, is defined by the integration of PDF of $g(\hat{d}, d)$,

$$P_f = \int_{g(\mathrm{x}) \leq 0} f(\mathrm{x})\,\mathrm{dx} \tag{24}$$

where $f(x)$ represents the joint probability density of the basic random variables, the random vector x contains all the uncertain variables, and $g(x)$ is the performance function corresponding to the considered failure mode.

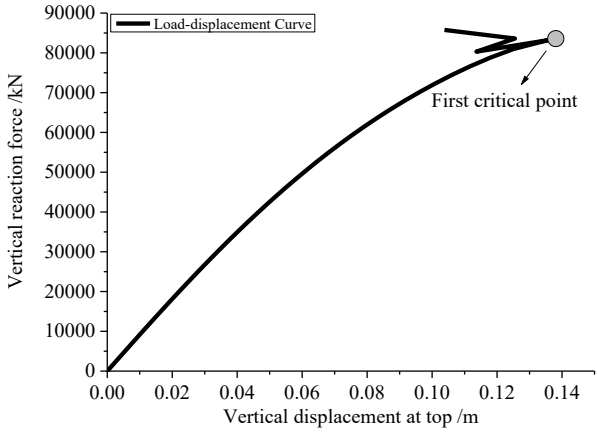

Fig. 9 Load–displacement curve

The specification of the appropriate safety level for the design is of special significance in engineering practice. In domes, the vertical stability is the governing factor. To evaluate the reliability of the dome, numerical approaches are first needed to evaluate the value of $\hat{d}$. Herein, the incremental vertical roof loads, which are assumed to be evenly distributed in the dome, are applied to all joints of the dome, and the vertical reaction force at the supports, and vertical deformation at the top of the dome can then be obtained, as shown in Fig. 9. Through the load–displacement curve, the collapse limit displacement due to the loss of stability is determined. In this paper, the load at the first critical point (peak value point or branch point) is considered as the ultimate load of the dome. It is observed that when the vertical deformation at the top is approximately 0.137 m, the limit state of the dome is reached. In general, the ultimate vertical deformation at the top is less than 1/300 of the span of a perfect dome when the collapse limit is reached. While the deformation at the top will be larger for the dome with imperfections, nevertheless, it is less than 1/250 of the span [43]. However, the dome subjected to complicated loads loses stability more easily than the one subjected to a single load. Therefore, in this paper, the selected threshold $\hat{d}$ is less than the ultimate displacement of 0.137 m for the purpose of safety. It is set to be 0.1 m for the domes with/without imperfections, which is approximately 75% of the ultimate displacement. Moreover, according to the curve, moderate nonlinearity is observed at a position of 0.1 m, where yielding of the dome begins to occur.

5.2 Generation of initial mode damping ratios

For the dome with the large span, the range of damping ratios of the entire structure is approximately 1–3%. One of the major problems encountered in dynamic analysis is the determination of damping ratios corresponding to higher modes. However, the results of field experiments indicate that the damping ratios of higher modes are difficult to be obtained. Because of limited experimental data, in order to obtain these damping ratios in this paper, the Rayleigh damping model that was proposed by Hall [44] is used to generate all the needed mode damping ratios. The form of the model is as following,

$$\alpha = 2\xi\hat{\omega}\frac{2R}{1+R+2\sqrt{R}} \tag{25}$$

$$\beta = 2\xi\frac{1}{\hat{\omega}}\frac{2}{1+R+2\sqrt{R}} \tag{26}$$

where R>1 and ξ is the first mode damping ratio. In order to consider the softening of the dome $\hat{\omega} = 0.667\omega_1$ in the cases where the initial stiffness matrix in Eq. (10) is used for a dynamic analysis. The parameters, ξ and R, are set to be equal to 0.025 and 1.4, respectively. Through the use of Eqs. (25) and (26), the damping coefficients, α and β, can be calculated, and the first 20 mode damping ratios are then generated for dynamic analyses through the use of Eq. (11).

After the generation, each mode damping ratio is assumed to obey the normal distribution, in which the mean of each damping ratio is equal to the value calculated based on Eq. (11), and in which a standard deviation is specified. In this paper, the damping ratio of each mode is randomly generated through the mean and the standard deviation, and the mass and stiffness damping coefficients are then calculated using Eq. (16).

5.3 Random variables in the dome and their deviations

In this paper, different distributions and standard deviations of random parameters are set and listed in Table 4. In the table, each random variable is uncorrelated. The standard deviations represent the variability levels of random variables. It is noted that, although the input parameters are random, they are bounded to avoid unrealistic values because of the control of construction quality.

Table 4 Uncertainty sources of the dome and their distributions

Uncertainty sources	Mean	Standard deviation	Probability distribution	Bounds
Elastic modulus /*MPa*	2.1e5	(0.03[a]/0.06[b]/0.1[c])*Mean	*Normal*	[1.9e5, 2.3e5]
Joint and support error /*m*	0	(0.05[a]/0.1[b]/0.2[c])	*Normal*	[-0.3, 0.3]
Member imperfection /*m*	0	(0.01[a]/0.03[b]/0.05[c])	*Normal*	[-0.03, 0.03]
Mode damping ratio	0.025	(0.1[a]/0.2[b]/0.3[c])*Mean	*Normal*	[0.015, 0.035]
[d]Dead load /*(kg/m^2)*	90	0.1*Mean	*Normal*	[72, 108]
[d]Live load /*(kg/m^2)*	36	0.5*mean	*Extreme value type I*	[18, 54]

Note: [a] Case 1, [b] Case 2, [c] Case 3; [d] In the analysis for the perfect structure, the factors of dead and live loads are set as 1.2 and 1.4, respectively.

5.4 Applied dynamic loads for dynamic analyses

In order to clearly present the dynamic behaviors of the dome with the developed method in this paper, the acceleration time series are designed using triangular functions as an example, and they are input at all nodes restrained in a specified direction with an uniform excitation method. Each time series includes three components, as illustrated in Fig. 10. The periods of the three components are respectively equal to 0.3 s, 0.3 s, and 0.4 s. The total duration is 8 s for each time series. The acceleration amplitudes (*cFactors*) and properties of dynamic loads are listed in Table 5, in which the phase shift is not included. The variability of the external excitations is not considered in this study.

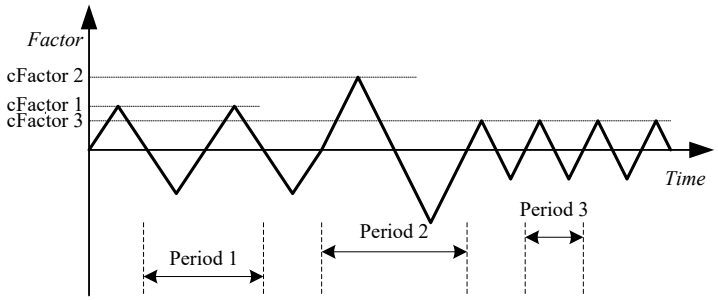

Fig. 10 Designed acceleration time series

Table 5 Properties of dynamic loads

Acceleration	cFactor 1	cFactor 2	cFactor 3	tStart	tEnd	Cycles	Period 1	Period 2	Period 3
Direction: *X*	0.4g	0.5g	0.05g	0s	8 s	1,1,9	0.3	0.3	0.4
Direction: *Y*	0.3g	0.4g	0.04g	0s	8 s	1,1,9	0.3	0.3	0.4
Direction: *Z*	0.24g	0.3g	0.03g	0s	8 s	1,1,9	0.3	0.3	0.4

6. Results and analyses

6.1 Random eigenvalue analyses

6.1.1 Dynamic property of the dome and its distribution

For a structure with a small damping, the natural frequency is an important characteristic and depends mainly on the two structural properties: stiffness, and mass. Compared with an ideal structure, its variance directly represents the changes of structural stiffness and/or mass distributions. Additionally, it has an important effect on structural dynamic demands of the structure, especially when subjected to earthquake ground motions because the structure may have a resonance with some frequency components in earthquake spectrums. Through single-random sampling, the first 20 natural frequencies of the dome are presented in Fig. 11. Through the sampling of a finite frequency, the distributions of natural frequencies of the dome of different cases are investigated. Fig. 12 shows the distributions of the first natural frequency of the dome using a sampling size equal to 100.

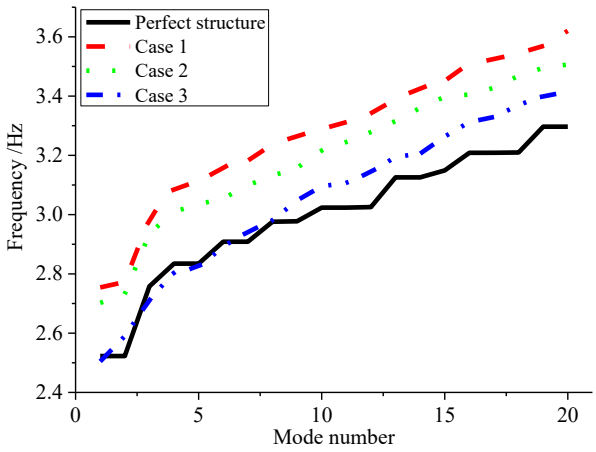

Fig. 11 Variation of the first twenty frequencies of the dome using single-random sampling

It is observed in Fig. 11 that the natural frequencies of the structure decrease to a certain extent with the increase of the standard deviations of the random variables. This indicates that the variance levels of the random variables have a negative effect on dynamic properties of the dome, because the reduction of the natural frequencies elicits the decrease of the stiffness when the distribution of the mass is constant. This results in structural flexibility and the reduction of the

carrying capacity of the dome. It can also be seen in Fig. 12 that the fundamental frequency (first mode frequency) obeys a normal distribution, and that the variability of the natural frequency increases with the increase of the variability levels of the random variables. However, in general, the standard deviations of the fundamental frequencies are very small in these normal distributions.

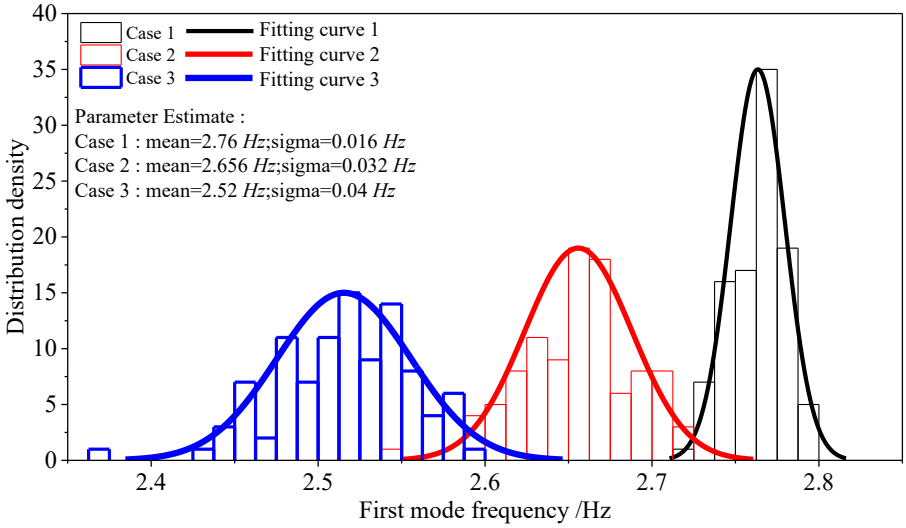

Fig. 12 Distributions of the first modal frequency using sample sizes equal to 50

6.1.2 Distributions of damping coefficients

Through random sampling over 100 times, the damping coefficients of different cases are calculated, as shown in Fig. 13. It can be seen that the damping coefficients are normally distributed. However, it should be noted that a large variability in damping coefficients is observed. In this paper, although the damping ratio of each mode has a variability, and the sample size for the damping ratio of each mode is limited, the use of LSM can reduce the errors of the damping coefficients estimated, and the LSM thus has robustness in predicting the damping coefficients. According to these mean damping coefficients,(α, β), and Eq. (11), the frequency-damping ratio curves can be obtained, as shown in Fig. 14. It is noted that although the difference of the frequency-damping ratio curves is small in different cases, the damping coefficients will be random in the single-sampling case, and this may lead to a significant difference in dynamic demands.

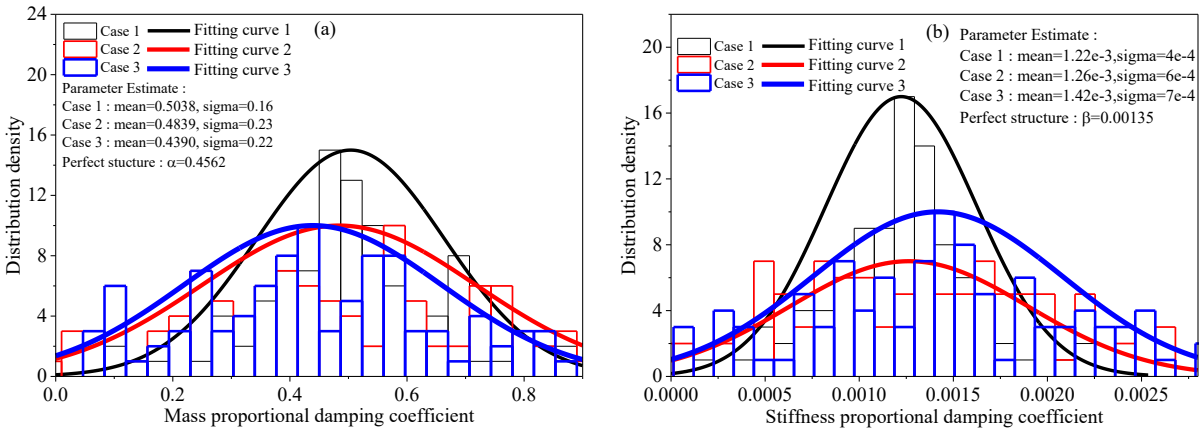

Fig. 13 Distributions of proportional damping coefficients for mass and stiffness

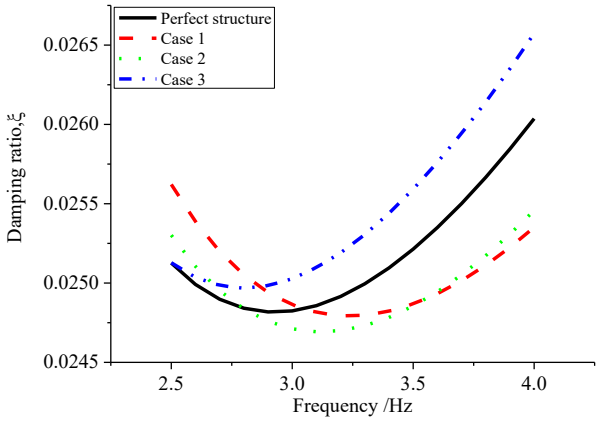

Fig.14 Generated frequency-damping ratio curves using the means of damping coefficients

6.2 Dynamic analyses

6.2.1 Dynamic responses and probabilities of failure of the dome

Through random sampling over 100 times, the statistical maximum vertical dynamic responses at the top are shown in Fig. 15. It is observed that all these responses generally obey the *lognormal* distribution. The distribution can be described using Eq. (27). Fitting the histogram yields the statistical parameters about all three cases, as listed in Table 6. Their means are respectively 0.0239 m, 0.0312 m, and 0.0384 m, while the maximum vertical dynamic response at the top is 0.0313m for the perfect dome. The probabilities of failure of the three cases are 0, 3e-4, and 7.8e-3, respectively. Therefore, it can be concluded that the variability levels of the input parameters have an important negative effect on the reliability of the dome. This suggests that reducing the uncertainty of the input parameters has a significant contribution to the safety of the domes. The CDFs of the three cases are shown in Fig. 16. It can be noted that the probabilities that the maximum vertical displacements are respectively larger than 0.06 m, 0.10 m, and 0.12 m are near zero among the three cases.

In engineering practice, estimating the dynamic reliability of a structural system has been a challenging aspect due to the mathematical description of the random input parameters, and the calculated workload. In this study, however, by means of a limited sampling size, the fitting technique for the performance function is used to approximately evaluate the reliability of the dome, and the computation complexity is thus reduced.

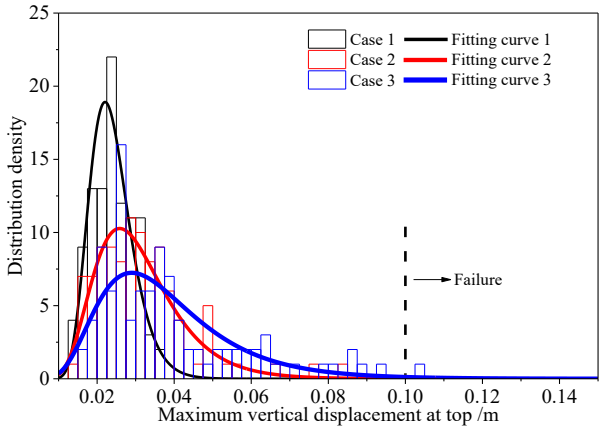

Fig. 15 statistical analyses of displacement

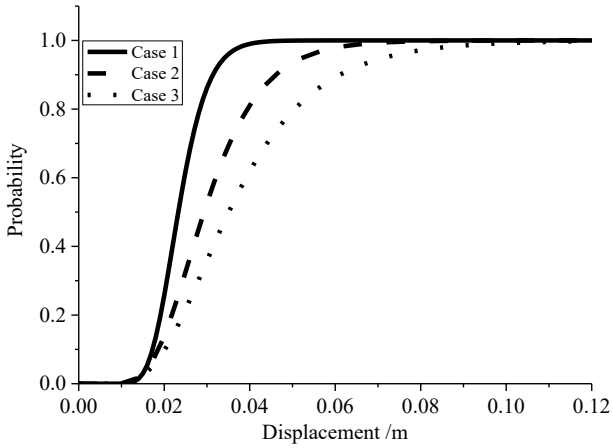

Fig.16 CDFs of displacement

$$f(\mu,\sigma)=\frac{1}{x\sigma\sqrt{2\pi}}\exp\left\{\frac{-(\ln x-\mu)^2}{2\sigma^2}\right\},\ x>0 \tag{27}$$

in which the $mean=exp\left\{\mu+\frac{\sigma^2}{2}\right\}$, and the variance is $var=exp(2\mu+\sigma^2)(exp(\sigma^2)-1)$.

Table 6 Parameter estimations and probability of failure of the dome

Case	μ	σ	Mean /m	Variance	P_f
1	-3.76	0.233	0.0239	3.18e-5	0.0
2	-3.53	0.353	0.0312	1.29e-4	3e-4
3	-3.35	0.433	0.0384	3.03e-4	7.8e-3

6.2.2 Damping force of the dome

In previous studies, discussion on the damping performance of a structure was limited, and there is still not a thorough understanding of the order of the magnitude of the damping force in a structure. Thus, the damping performance of the structure cannot be assessed. However, the damping performance is noneligible in performance-based seismic designs because it is an important energy dissipation part in a structure. In this study, the maximum vertical damping forces at the top of the dome in the three cases studied are investigated, as shown in Fig. 17. Through a statistical analysis, it is observed that these damping forces obey the *lognormal* distribution, and the statistical parameters of PDFs are listed in Table 7. In the table, the means of the maximum vertical damping forces have an order of amplitude of approximately 2–3 kN, and increase with the increase of the variability levels of the random input parameters, while the maximum vertical damping force at the top is 3.87 kN for the perfect dome. Their CDFs are shown in Fig. 18. This shows that the probabilities that the maximum vertical damping force at the top is larger than 4 kN, 7 kN, and 10 kN are equal to zero among the three cases.

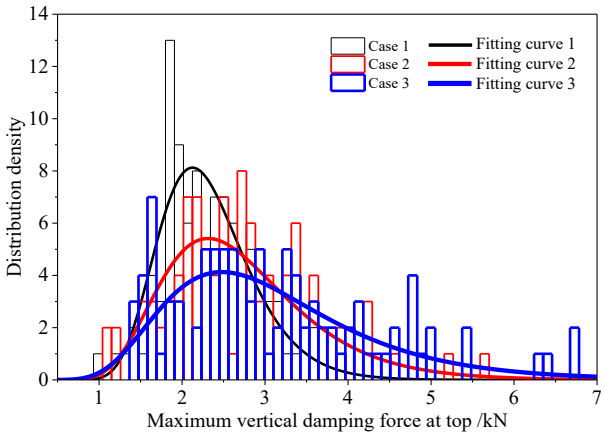

Fig. 17 Statistical analyses of damping force

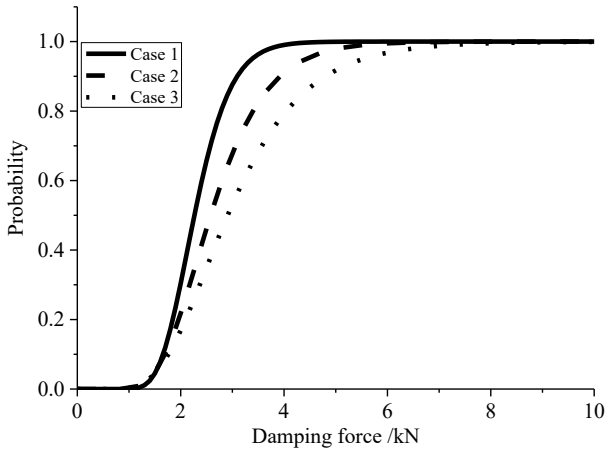

Fig.18 CDFs of damping forces

Table 7 Distribution parameters of damping force

Case	μ	σ	Mean /*kN*	Variance
1	-6.09	0.243	2.32	3.28e-7
2	-5.96	0.327	2.72	8.33e-7
3	-5.84	0.391	3.12	1.61e-6

6.3 A comparative study of the domes with and without uncertainties

In a single-sampling case, one sample is selected at random from every variable from their individual sampling space.

This group of data from single sampling represents a potential case of a structure. This can present the uncertainties of dynamic demands, and the entire effect of all random variables on dynamic demands. In this paper, the uncertainties of forces and deformations are discussed using two single-sampling schemes. Considering three typical members M-1 (hoop member), M-2 (ridge member), and M-3 (diagonal member), shown in Fig.7(b), as an example, the relationships between the axial reaction forces and vertical deformations at mid-span in different cases are shown in Figs. 19 to 21.

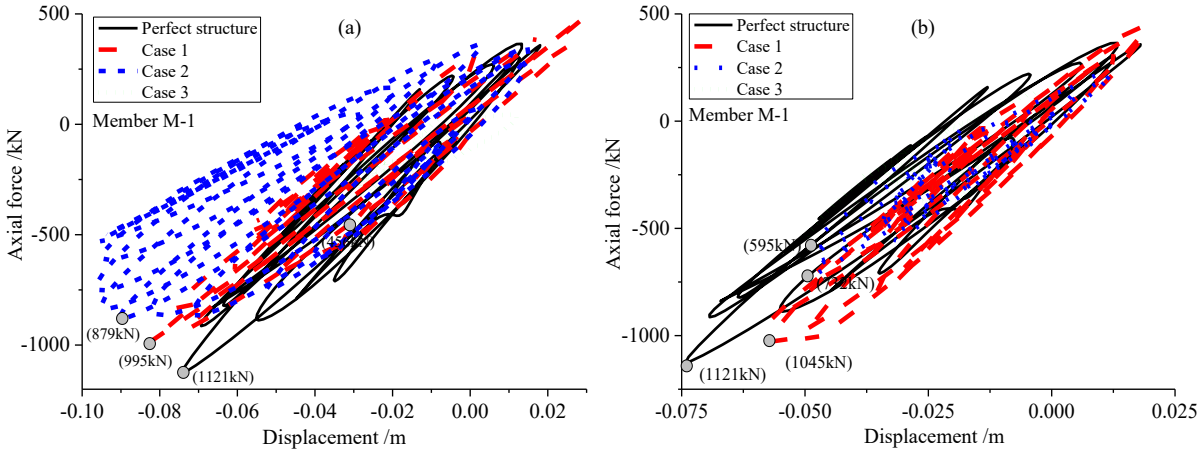

Fig. 19 Axial force–deformation curves of the member M-1 (hoop member)

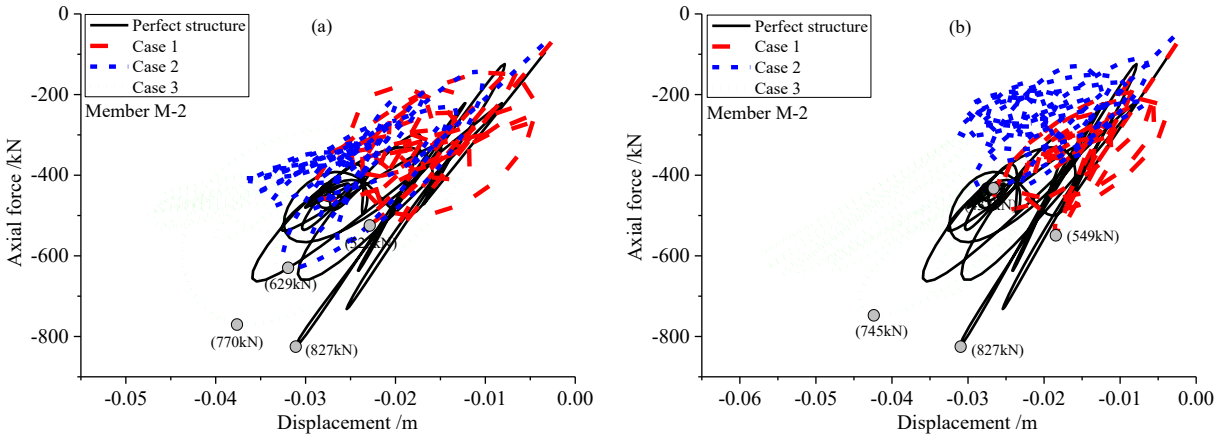

Fig. 20 Axial force–deformation curves of the member M-2 (ridge member)

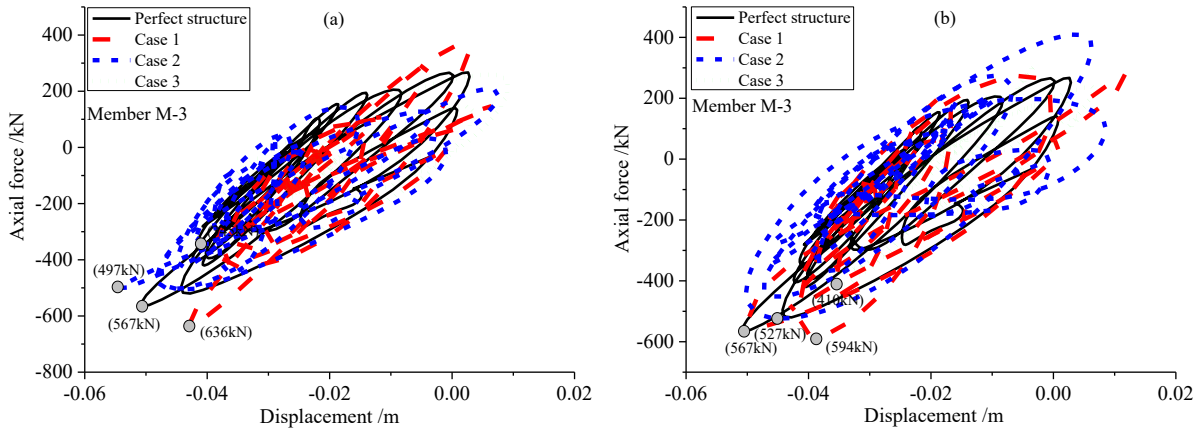

Fig. 21 Axial force–deformation curves of the member M-3 (diagonal member)

It can be seen that these members are mainly subjected to the axial pressure force. In general, as the variability levels of the random variables increase, the maximum axial reaction force decreases. This indicates that the contribution of the

members to the carrying capacity of the domes reduces. As expected, the reduction of the variability levels of the random input variables can improve the structural performance. Compared to the perfect dome, the axial reaction forces of the members in the dome with uncertain input parameters are less than the one in the dome with specific input parameters. There are, however, some exceptions, such as the axial forces in Fig. 21. In addition, a large difference in responses can also be observed in these figures. Therefore, the conventional method for a dynamic analysis may give rise to large errors in predicting the dynamic demands of the dome.

7. Conclusions

In this paper, a comprehensive dynamic analytical procedure with multisource random variables is presented based on the finite element method. Damping, material, geometry, and load parameters are simultaneously taken into account in these analyses. The treatments of uncertainty in damping are proposed, where the material damping is modeled by the Bouc–Wen material model and the structural damping is modeled using the Rayleigh damping model. In Rayleigh damping model, the damping coefficients are calculated using the LSM that has a high accuracy and robustness. Dynamic reliability analysis of a dome is performed. Such analysis indicates that the variance level of the random variable has a negative effect on the dynamic properties and safety of the dome, and that the structural dynamic responses and damping forces obey the $lognormal$ distribution. It has an order of amplitude of less than 10 kN in damping forces under the current external excitations. Through a comparison between the perfect dome and the one with uncertain input parameters, the obvious difference in dynamic demands is observed. Numerical results in this paper also reveal the necessity for the method proposed.

Data Availability

The data used to support the findings of this study are available from the corresponding author upon request.

Conflicts of Interest

The author declares that there are no conflicts of interest regarding the publication of this paper.

Acknowledgements

The authors would like to gratefully acknowledge the financial support provided by the National Natural Science Foundation of China (Grant No.: 51108301).

References

1. K. K. Choi, and J. L. T. Santos, “Design sensitivity analysis of non-linear structural systems, Part I: Theory,” *Int J Numer Meth Eng*, vol. 24, no. 11, pp. 2039–2055, 2010.
2. Y. Zhang, and A. Der Kiureghian, “Dynamic response sensitivity of inelastic structures,” *Comput Methods Appl Mech Eng*, vol. 108, no. 1–2, pp. 23–36, 1993.
3. T. Haukaas, and A. Der Kiureghian, “Finite element reliability and sensitivity methods for performance-based engineering,” Tech. Rep., Berkeley (CA): Pacific Earthquake Engineering Research Center, University of California, 2004.
4. A. Der Kiureghian, “Analysis of structural reliability under parameter uncertainties,” *Probabilistic Eng Mech*, vol. 23, no. 4, pp. 351–358, 2008.
5. H. S. Lee, J. W. Shin, M. Park, and H. G. Ryu, “Probabilistic duration estimation model for high-rise structural work,”*J of Constr Eng and Manag*, vol. 135, no. 12, pp. 1289–1298, 2009.
6. T. Haukaas, and M. H. Scott, “Shape sensitivities in the reliability analysis of nonlinear frame structures,” *Comput and Struct*, vol. 84, no.15-16, pp. 964–977, 2006.
7. A. Der Kiureghiana, and O. Ditlevsen, “Aleatory or epistemic? Does it matter?,” *Struct Saf*, vol. 31, no. 2, pp. 105–112, 2009.

8. H. G. Matthies, “Quantifying uncertainty: modern computational representation of probability and applications,” in Proceedings of the *extreme Man-Made and Natural Hazards in Dynamics of Structures(NATO Security through Science Series)*, pp. 105–135, 2007.
9. P. E. Hess, and D. Bruchman, I. A. Assakkaf, and B. M. Ayyub, “Uncertainties in material and geometric strength and load variables,” *Nav Eng J*, vol. 114, no. 2, pp. 139–166, 2010.
10. I. Vryzidis, G. Stefanou, and V. Papadopoulos, “Stochastic stability analysis of steel tubes with random initial imperfections,” *Finite Elem in Anal & Des*, vol. 77, no. 77, pp. 31–39, 2013.
11. M. Alembagheri, and M. Seyedkazemi, “Seismic performance sensitivity and uncertainty analysis of gravity dams,” *Earthquake Engng Struct Dyn*, vol. 44, no. 1, pp. 41–58, 2015.
12. J. M. T. Thompson, and G. W. Hunt, “On the buckling and imperfection-sensitivity of arches with and without prestress,” *International J of Solids and Struct*, vol. 19, no. 5, pp. 445–459, 1983.
13. H. A. Mang, C. Schranz, and P. Mackenzie-Helnwein, “Conversion from imperfection-sensitive into imperfection insensitive elastic structures I: Theory,” *Comput Methods in Appl Mech and Eng*, vol. 195, no. 13-16, pp. 1422–1457, 2006.
14. C. A. Schenk, and G. I. Schueller, “Buckling analysis of cylindrical shells with random geometric imperfections,” *Int J Non-Linear Mech*, vol. 38, no. 7, pp. 1119–1132, 2003.
15. V. Papadopoulos, and P. Iglesis, “The effect of non-uniformly axial loading on the buckling behavior of shells with random imperfections,” *Int J of Solids and Struct*, vol. 44, no. 18, pp. 6299–6217, 2007.
16. D. Schillinger, V. Papadopoulos, M. Bischoff, and M. Papadrakakis, “Buckling analysis of imperfect I-section beam-columns with stochastic shell finite elements,” *J Comput Mech*, vol. 46, no. 3, pp. 495–510, 2010.
17. American Institute of Steel Construction, “ANSI/AISC 360-10 specification for structural steel buildings,” Chicago, IL, 2010.
18. V. Papadopoulos, and M. Papadrakakis, “Finite element analysis of cylindrical panels with random initial imperfections,” *J of Eng Mech (ASCE)*, vol. 130, no. 8, pp. 867–876, 2004.
19. E. Bielewicz, and J. Gorski, “Shells with random geometric imperfections simulation-based approach,” *Int J of Non-Linear Mech*, vol. 37, no. 4–5, pp. 777–784, 2002.
20. A. P. Smith, J. Garloff, and H. Werkle, “Verified solution for a statically determinate truss structure with uncertain node locations,” *J of Civ Eng and Archit*, vol. 4, no. 11, pp. 1–10, 2010.
21. T. Haukaas, and A. Der Kiureghian, “Parameter sensitivity and importance measures in nonlinear finite element reliability analysis,” *J Eng Mech*, vol. 131, no. 10, pp. 1013–1026, 2005.
22. J. K. Guest, and T. Igusa, “Structural optimization under uncertain loads and nodal locations,” *Comput Methods in Appl Mech and Engineering*, vol. 198, no. 1, pp. 116–124, 2008.
23. B. R. Ellingwood, T. V. Galambos, J. G. MacGregor, and C. A. Cornell, “Development of probability based load criterion for American national standard A58,” Tech. Rep., Faithersburg (MD): National Bureau of Standard Special Publication, 1980.
24. R. Corotis, and V. Doshi, “Probability models for live load survey results,” *J of the Struct Div (ASCE)*, vol. 103, no. 6, pp. 1257–1274, 1977.
25. E. Choi, “Live load for Office Buildings: effect of occupancy and code comparison,” *J of Struct Eng (ASCE)*, vol. 116, no. 11, pp. 3162–3174, 1990.
26. W. M. Bulleit, “Uncertainty in structural engineering,” *Pract Period on Struct Des and Constr*, vol. 13, no. 1, pp. 24–30, 2008.
27. H. D. Zhang, and Q. H. Han, “A numerical investigation of seismic performance of large span single-layer latticed domes with semi-rigid joints,” *Struct Eng and Mech*, vol. 48, no. 1, pp. 57–75, 2013.
28. A. Kareem, and K. Gurley, “Damping in structures: its evaluation and treatment of uncertainty,” *J of Wind Eng and Ind Aerodyn*, vol. 59, no. 2, pp. 131–157, 1996.
29. A. Kareem, W. J. Sun, “Dynamic response of structures with uncertain damping,” *Eng Struct*, vol. 12, no. 1, pp, 2–8, 1990.
30. Y. K. Wen, “Method for random vibration of hysteretic systems,” *J of the Eng Mech Div*, vol. 102, no. 2, pp. 249–263, 1976.
31. T. T. Baber, and M. N. Noori, “Random vibration of degrading pinching systems,” *J of Eng Mech (ASCE)*, vol. 111, no. 8, pp.

1010–1026, 1985.

32. F, Ma, H. Zhang, and A. Bockstedte, G. C. Foliente, and P. Paevere, “Parameter analysis of the differential model of hysteresis,” *J of Appl Mech (ASME)*, vol. 71, no. 3, pp. 342–349, 2004.
33. F. A. Charney, “Unintended consequences of modeling damping in structures,” *J of Struct Eng*, vol. 134, no. 4, pp. 581–592, 2008.
34. L. E. Goodman, *Material damping and slip damping (in shock and vibration handbook)*, McGraw-Hill, NY, USA, 2002.
35. H. D. Zhang, Y. F. Wang, and Q. H. Han, “Nonlinear material loss factors of single-layer latticed domes subjected to earthquake ground motions,” *J Struct Eng*, vol. 141, no. 7, 04014181, 2014.
36. J. F. Semblat, “Rheological interpretation of Rayleigh damping,” *J of Sound and Vib*, vol. 206, no. 5, pp. 741–744, 1997.
37. Architectural Institute of Japan (AIJ) , “Damping of buildings,” Tech. Rep., Japan, 2000.
38. Y. Tamura, “Damping in buildings,” Lecture, Tokyo Polytechnic University, 2008.
39. M. Raffy, and C. Gontier, “Statistical error on damping ratios in deterministic subspace identification,” in *Proceedings of the 21st IMAC Conference and Exposition 2003 (IMAC XXI): A Conference and exposition on structural dynamics*, Kissimmee, Florida, 2003.
40. B. K. Low, and W. H. Tang, “Efficient spreadsheet algorithm for first-order reliability method,” *J of Eng Mech (ASCE)*, vol. 133, no. 12, pp. 1378–1387, 2007.
41. A. Der Kiureghian, H. Z. Lin, and S. J. Hwang, “Second-order reliability approximations,” *J of Eng Mech (ASCE)*, vol. 113, no. 8, pp.1208–1225, 1987.
42. W. Zhou, H. P. Hong, “System and member reliability of steel frames,” *Steel and Compos Struct*, vol. 4, no. 6, pp. 419–435, 2004;.
43. Z. G. Cao, F. FAN, S. Z. Shen, “Elasto–plastic stability analysis of single-layer latticed domes,” *Eng Mech*, vol. 15, no. 5, pp.881–884, 2007.
44. J. F. Hall, “Problems encountered from the use (or misuse) of Rayleigh damping,” *Earthq Eng & Struct Dyn*, vol. 35, no. 5, pp. 525–545, 2006.